Pharmaceutical Sciences and Drug Design
ISSN: 3062-4428
2023, Volume 3, Page No: 86-97

Available online at: www.galaxypub.co/page/journals

Galaxy Publication

Galaxy Publication

Repositioning Nitrofurantoin for Breast Cancer Treatment Using Cubosome-Based Delivery Systems

Emma Wright[1]*, Chloe Adams[1]

[1]Department of Phytochemistry, Faculty of Pharmacy, University of Zurich, Zurich, Switzerland

***E-mail** ✉ emma.wright.ch@gmail.com

Received: 09 January 2023; **Revised:** 11 March 2023; **Accepted:** 11 March 2023

ABSTRACT

Nitrofurantoin (NITRO), a well-established antibiotic for urinary tract infections, is activated by nitroreductases, a mechanism that has prompted its investigation for repurposing in breast cancer treatment, as these cancers express the nitroreductase gene.NITRO-loaded cubosomes were prepared via hot homogenization following a 2^3 full factorial design. Variables examined included the drug-to-oil phase ratio (1:10 and 2:10), oil-to-aqueous phase ratio (1:10 and 1:5), and Glyceryl mono-oleate (GMO) to Poloxamer 407 (PX407) ratio (0.25:1 and 0.5:1). Eight formulations were developed and characterized for particle size, zeta potential, polydispersity index, and entrapment efficiency.Formulation S6 (1:10 drug-to-oil, 1:5 oil-to-aqueous, 0.5:1 GMO:PX407) demonstrated the highest desirability, with a particle size of 45.5 ± 1.1 nm and entrapment efficiency of 98.6 ± 1.8%, and was selected for further studies. TEM analysis confirmed its morphology. The intracellular cytotoxicity of S6 against MCF-7 breast cancer cells was assessed via MTT assay, revealing a significantly lower IC50 (83.99 ± 0.15 µg/mL) compared to free NITRO (174.54 ± 1.36 µg/mL), indicating enhanced anticancer efficacy.Nitrofurantoin-loaded cubosomes show promise for repurposing in breast cancer therapy, warranting further stability testing and in vivo evaluation.

Keywords: Factorial design, Glyceryl monooleate, Nitro reductase, MTT assay, Poloxamer 407

How to Cite This Article: Wright E, Adams C. Repositioning Nitrofurantoin for Breast Cancer Treatment Using Cubosome-Based Delivery Systems. Pharm Sci Drug Des. 2023;3:86-97. https://doi.org/10.51847/2sJGnmkDcG

Introduction

Cancer is a complex, multifactorial disease characterized by uncontrolled cell proliferation and continuous genomic alterations, resulting in the transformation of normal cells into malignant ones [1, 2]. The primary objective of cancer therapy is to inhibit tumor growth, prevent metastasis, and reduce recurrence after treatment, thereby extending patient survival [3]. Conventional treatments, including surgery, chemotherapy, and radiotherapy, face limitations such as treatment resistance, severe side effects, and lack of targeted delivery [4], often leading to suboptimal outcomes and prompting the search for novel therapeutic strategies [5].

According to the World Health Organization, approximately 2.3 million women were diagnosed with breast cancer in 2020, with around 0.5 million deaths reported annually [6, 7]. Common treatments include radiotherapy [8] and various chemotherapeutic agents [9]. Nanocarrier-based drug delivery has emerged as a promising approach in cancer therapy [10], involving platforms such as liposomes, polymeric nanoparticles, polymeric micelles, dendrimers [11], magnetic nanoparticles [12], and pH-sensitive nanovehicles [13]. Additionally, photodynamic therapy, which uses laser light, has been recognized as an effective and patient-friendly treatment option, with femtosecond lasers being explored for enhanced cancer therapy [14, 15].

Drug repositioning refers to the application of an existing drug for a new therapeutic indication, offering a cost- and time-efficient alternative to novel drug development. It benefits from pre-existing pharmacokinetic and safety data, reducing the need for extensive early-stage testing [16].

Nitrofurantoin (NITRO), a nitrofuran derivative (1-[(E)-(5-nitrofuran-2-yl)methylideneamino]imidazolidine-2,4-dione) synthesized from hydantoin, is traditionally used to prevent and treat urinary tract infections. Its mechanism

involves inhibition of bacterial DNA synthesis through nitroreductase-mediated reduction of the nitro group, forming reactive intermediates and hydroxyl radicals that damage DNA [17–19]. Recent studies suggest that NITRO also exerts cytotoxic effects on tumor cells expressing nitroreductases [5], with in vitro evidence demonstrating inhibition of various cancer cell lines, including colon, prostate, and breast cancers [20]. Nitro compounds exhibiting enzymatic nitro-group reduction can interact with essential cellular biomolecules, conferring selective anticancer activity, particularly in hypoxic solid tumors [21, 22].

Nitrofurantoin is classified as a Biopharmaceutics Classification System class IV drug, characterized by poor solubility and low permeability [23]. Enhancing its bioavailability requires carrier systems capable of improving solubility and absorption. Nanotechnology has greatly advanced cancer therapeutics by improving drug delivery efficiency, enhancing pharmacokinetics, enabling tumor-specific targeting, reducing toxicity, and overcoming resistance [24, 25]. Nanomaterials such as gold, silver, and copper also show significant potential in cancer diagnostics through immunosensor applications [26].

Lipid-based nanoparticles play a key role in improving both solubility and permeability of drugs. Among these, cubosomes—lipid-based liquid crystalline nanoparticles—are widely used for drug delivery in cancer therapy [27, 28]. Cubosomes provide tunable membrane curvature independent of particle size, allowing targeted delivery, prolonged circulation, and sustained drug release [28]. These self-assembled nanoparticles are typically derived from bi-continuous cubic-phase lipids like Glyceryl Mono-oleate (GMO), stabilized by Pluronics, although Phytantriol can also be used in cosmetic formulations [29, 30]. Their bi-continuous honeycomb structure allows high drug-loading capacity [31–33], and they can be prepared using top-down or bottom-up methods [34, 35]. Compared to liposomes, cubosomes better accommodate hydrophobic drugs, and their characterization involves electron microscopy, X-ray scattering, particle size, and entrapment efficiency assessments [36, 37].

The small size of cubosomes improves drug permeation and retention at tumor sites, fulfilling a critical requirement for cancer therapy [37]. They also enable higher drug loading and lower viscosity, with the capacity to incorporate water-soluble drugs within their bilayers. Upon enzymatic digestion, these cubosomes form bioadhesive particles with prolonged intestinal contact, enhancing absorption and bioavailability [38–40]. Cubosomes are versatile carriers with theranostic potential and can be administered orally, topically, or intravenously. Recent advancements have optimized their preparation, targeting, drug release control, and efficacy. Cubosomes have been successfully employed to deliver anticancer agents including 5-Fluorouracil, Cisplatin, Paclitaxel, Temozolomide, Doxorubicin, and Icarin to various cancer cells [28, 41].

In this study, NITRO is explored for repurposing in breast cancer therapy targeting cells expressing nitroreductases necessary for its activation. Formulation as cubosomes aims to exploit their unique drug delivery properties to enhance the therapeutic efficacy of NITRO.

Materials and Methods

Materials

Nitrofurantoin (NITRO) was kindly provided by Sinochem Jiangsu, China. Poloxamer 407 (PX407) was obtained from Fisher Scientific, UK, while Glyceryl monooleate (GMO, 90–95%) and dimethyl formamide (DMF) were purchased from Sigma Aldrich, USA. All other reagents used were of analytical grade.

Methods

Preparation of NITRO-Loaded Cubosomes (NITRO-Cs)

The lipid (oily) phase of the cubosomes, composed of PX407 and GMO, was weighed according to the designated ratios and melted in a hot water bath at 60 °C to form a uniform dispersion. The molten lipid mixture was thoroughly stirred before adding the accurately weighed amount of NITRO. The resulting dispersion was subjected to high-speed homogenization (Heidolph Diax 900, Germany) at 10,000 rpm for 10 minutes, during which preheated distilled water (60 °C) was added dropwise. This was followed by a 2-minute probe sonication (GE 130, China) applied in 2-second pulses to break up any agglomerates. The prepared NITRO-Cs were then allowed to cool and stored in amber glass vials for 48 hours prior to further evaluation [42].

Full factorial design

A 2^3 full factorial experimental design was implemented using Design-Expert VR software (V.7.0.0, Stat-Ease Inc., Minneapolis, USA) to examine the influence of three independent variables on the cubosome characteristics.

The factors studied were the drug-to-oil phase ratio (X1), oil-to-aqueous phase ratio (X2), and GMO-to-PX407 ratio (X3). The responses measured included particle size (PS, R1), zeta potential (ZP, R2), polydispersity index (PDI, R3), and percentage entrapment efficiency (%EE, R4). Optimization aimed to minimize PS and PDI while maximizing ZP and %EE to achieve the formulation with the highest desirability. **Table 1** summarizes the factors, their levels, and the constraints applied during the preparation and optimization of NITRO-Cs.

Table 1. 2^3-Factorial Design Independent Variables, Their Levels, Responses and Constraints for NITRO-Cs Systems

Factors (Independent Variables)	**Levels**	
	Minimum	**Maximum**
Drug: Oily phase ratio (X1)	1:10	2:10
Oily: Aqueous phase ratio (X2)	1:10	1:5
GMO: PX 407 ratio (X3)	0.25:1	0.5: 1
Responses	**Constraints**	
R1: Particle Size (PS)	Minimize	
R2: Zeta Potential (ZP)	Maximize	
R3: Polydispersity Index (PDI)	Minimize	
R4: Percentage entrapment efficiency (%EE)	Maximize	

Evaluation of NITRO-Cubosomes (NITRO-Cs)

Entrapment efficiency (%EE)

The entrapment efficiency was quantified using an established indirect approach [43]. To separate the free drug from the cubosomes, NITRO-Cs formulations were centrifuged (Cooling Centrifuge, Centurion Scientific K3 Series, Germany) [44]. Two-milliliter samples were placed in Eppendorf tubes and spun at 14,000 rpm at 4°C for 10 minutes, which caused the cubosomes to precipitate while leaving the unencapsulated drug in the aqueous supernatant. One milliliter of the resulting supernatant was diluted to 25 mL with distilled water, and its absorbance was measured at 375 nm using a UV spectrophotometer (Lab India UV-320, Mumbai, India) [45]. The concentration of free NITRO in the supernatant was then calculated from a calibration curve previously prepared in distilled water. Each system was analyzed six times, and the amount of drug encapsulated in the cubosomes was determined using the following equation:

$$\%EE = \frac{C_{total} - C_{free}}{C_{total}} \times 100 \quad (1)$$

Where C_{free} represents the measured concentration of un-entrapped NITRO and C_{total} is the total amount of NITRO present in 1 mL of cubosome dispersion.

Particle Size (PS), Zeta Potential (ZP), and Polydispersity Index (PDI)

The average particle size, PDI, and ZP of the NITRO-Cs formulations were evaluated using laser diffraction via a Zetasizer (Malvern Nano Series ZS90, Malvern Instruments, Ltd., Worcestershire, UK). Samples of 0.5 mL were diluted with 30 mL of distilled water to achieve optimal scattering intensity. All measurements were performed at 25°C [46, 47].

In-Vitro release study

The release profile of the optimized cubosome formulation was assessed using a dialysis membrane method (Dialysis Tubing Cellulose Membrane, MWCO 12,000–14,000, SERVA GmbH, Heidelberg, Germany) [48]. One milliliter of the selected formulation (17 mg/mL) or an equivalent amount of free NITRO in 1 mL PBS (pH 7.4) was placed into a tube sealed with the dialysis membrane. The tube was immersed in 50 mL of PBS (pH 7.4) at 37 ± 0.5°C under stirring at 150 rpm. Samples (3 mL) were withdrawn at 0.5, 1, 2, 3, 4, 5, 6, and 12 hours and replaced with an equal volume of fresh buffer. Withdrawn aliquots were diluted appropriately and the drug content was determined spectrophotometrically at 375 nm. Experiments were conducted in six replicates, and the percentage of drug release was calculated as the ratio of released drug to the initial drug amount in the dialysis

tube. Release profiles of free NITRO and the optimized formulation were compared at 4 and 8 hours, with statistical significance analyzed using Student's t-test.

Transmission Electron Microscopy (TEM)

The morphology of the optimized NITRO-Cs formulation was visualized using TEM (JEOL, JEM-1400, Japan) [49]. A drop of the diluted cubosome suspension was placed on a carbon-coated copper grid and stained with 1% sodium phosphotungstate, then air-dried at room temperature before imaging at 200 kV.

Cytotoxicity assessment using MCF-7 cells

The cytotoxic potential of the optimized NITRO-Cs formulation was evaluated on MCF-7 human breast cancer cells (VACSERA, Egypt; sub-cultured from ATCC® HTB-22™) using the MTT assay [50]. Cells were seeded in 96-well plates at 1×10^5 cells/mL and incubated at 37°C for 24 hours to form a confluent monolayer in RPMI-1640 medium supplemented with 1% L-glutamine, 10% inactivated fetal bovine serum, 50 µg/mL gentamycin, and HEPES buffer. The optimized cubosomes were compared to free NITRO and unloaded cubosomes, with serial dilutions prepared in RPMI with 2% serum (31.25–1000 µg/mL). Aliquots of 0.1 mL were added to wells in quintuplicate, with two wells as controls. Plates were incubated at 37°C, and cells were monitored for morphological changes such as rounding, monolayer disruption, granulation, or shrinkage. Subsequently, 20 µL of 5 mg/mL MTT solution was added to each well, shaken at 150 rpm for 5 minutes, and incubated for 4 hours at 37°C, 5% CO2. Formazan crystals were dissolved in 200 µL DMSO, mixed thoroughly, and absorbance was measured at 560 nm with background subtraction at 620 nm using a Biotek ELX800 microplate reader. Cell viability was directly proportional to optical density.

Statistical analysis

Data analysis and optimization were performed using Design-Expert VR software (V.7.0.0, Stat-Ease Inc., Minneapolis, USA) and Microsoft Excel 2019. Full factorial ANOVA was used to compare means at $p < 0.05$, followed by Tukey's post hoc test. Numerical optimization was carried out according to the constraints in **Table 2** [51]. All experiments were repeated six times, with results presented as mean ± SD.

Table 2. Composition and results of characterization of NITRO-Cs systems

S	Drug: Oily phase ratio (X1)	Oily: Aqueous phase ratio (X2)	GMO: PX407 ratio (X3)	PS (nm) (R1)	ZP (mV) (R2)	PDI (R3)	%EE (R4)
1	2:10	1:10	0.25:1	89.9±1.7	−19.4± 2.8	0.6± 0.0	98.7±1.9
2	1:10	1:5	0.25:1	34.5±0.1	−15.9±0.1	0.3± 0.0	98.6± 1.8
3	1:10	1:10	0.25:1	50.5±1.6	−16.1±0.4	0.5± 0.1	97.4±1.0
4	1:10	1:10	0.5:1	72.9±0.1	−7.9±2.2	0.4± 0.0	98.0±1.4
5	2:10	1:10	0.5:1	57.7±0.4	−8.2 ±0.8	0.4± 0.1	98.3±1.6
6	1:10	1:5	0.5:1	45.5±1.1	−13.4±0.6	0.3± 0.0	98.6±1.8
7	2:10	1:5	0.5:1	50.9±3.9	−23.8±1.4	0.4± 0.0	98.1±1.4
8	2:10	1:5	0.25:1	52.9±2.1	−8.6 ± 0.7	0.6± 0.1	97.9± 1.3

Results and Discussion

All prepared NITRO-C formulations appeared as uniform milky-yellow dispersions without any signs of aggregation. Based on the experimental design, eight NITRO-loaded cubosome systems were evaluated, and their composition, along with characterization results, are summarized in **Table 2**.

Analysis of variance revealed that particle size (PS) was significantly influenced by all examined factors, including the drug-to-oily phase ratio, the oily-to-aqueous phase ratio, and the GMO-to-PX407 ratio ($p = 0.0006$). Smaller particle sizes were favored by lower drug-to-oily phase ratios, higher oily-to-aqueous phase ratios, and higher GMO-to-PX407 ratios.

Zeta potential (ZP) was also significantly affected by the studied variables ($p = 0.0141$), with increases in drug-to-oily phase ratio, oily-to-aqueous phase ratio, and GMO-to-PX407 ratio corresponding to higher ZP values. Similarly, the polydispersity index (PDI), representing particle size distribution, was significantly influenced by the formulation variables ($p < 0.0001$). Lower PDI values were observed with lower drug-to-oily phase ratios, higher oily-to-aqueous phase ratios, and higher GMO-to-PX407 ratios.

Figure 1 presents the interactions among these formulation variables and their combined effects on PS, ZP, and PDI.

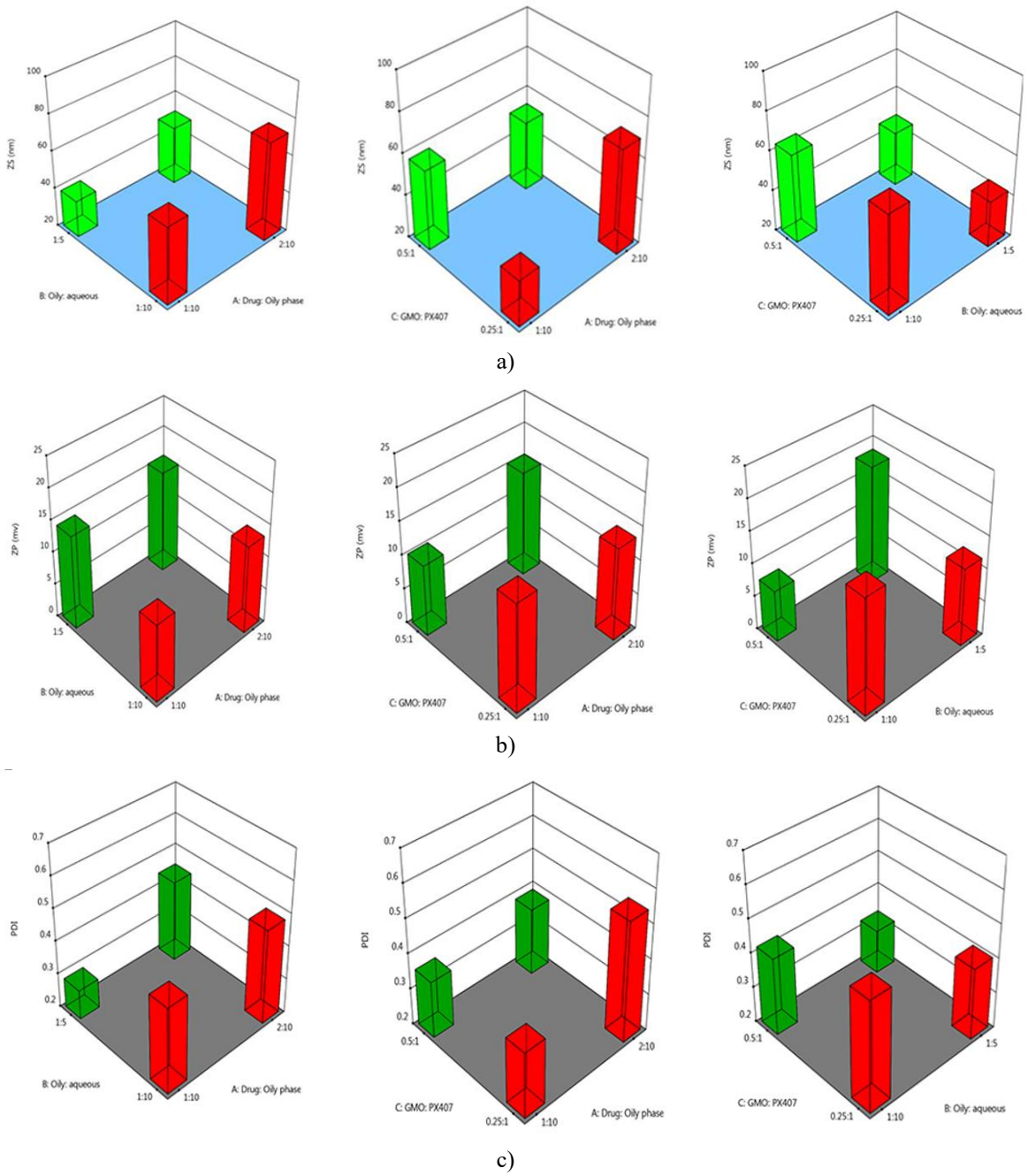

Figure 1. Effects of interactions among the studied formulation variables on Nitrofurantoin cubosome system particle size (PS, a), zeta potential (ZP, b), and polydispersity index (PDI, c).

Numerical optimization was performed using the desirability approach based on the factorial design data, aiming to identify the values of X1, X2, and X3 that would minimize PS and PDI while maximizing ZP and %EE. Desirability scores range from 0 (undesirable) to 1 (most desirable). The analysis identified system S6 as the

optimized formulation, with the highest desirability value of 0.774. The composition of S6 included a 1:10 drug-to-oily phase ratio, a 1:5 oily-to-aqueous phase ratio, and a 0.5:1 GMO-to-PX407 ratio.
System S6 was subsequently selected for further studies, including evaluation of its in vitro drug release profile. **Figure 2** depicts the release of Nitrofurantoin from S6 in comparison to the free drug.

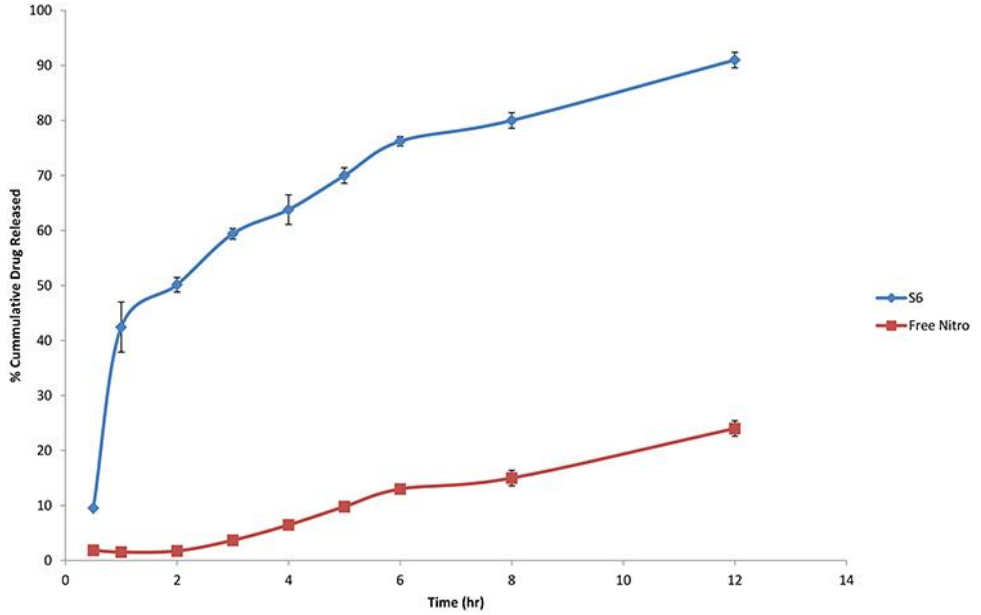

Figure 2. Cumulative percentage of Nitrofurantoin released from the S6 formulation compared to the free drug. The results demonstrate a significantly enhanced release from S6, with differences observed at 4 hours ($p = 0.00055$) and 8 hours ($p = 0.000237$).

Kinetic modeling of S6 drug release indicated a zero-order release pattern, with $R^2 = 0.8929$ for zero-order kinetics, $R^2 = 0.4689$ for first-order, and $R^2 = 0.889$ for the Higuchi model.
Transmission electron microscopy (TEM) images of S6 **(Figure 3)** revealed cubosomes with spherical to polygonal shapes. The particles exhibited a distinct dark outer coat and a lighter core containing the encapsulated drug, with sizes appearing below 50 nm.

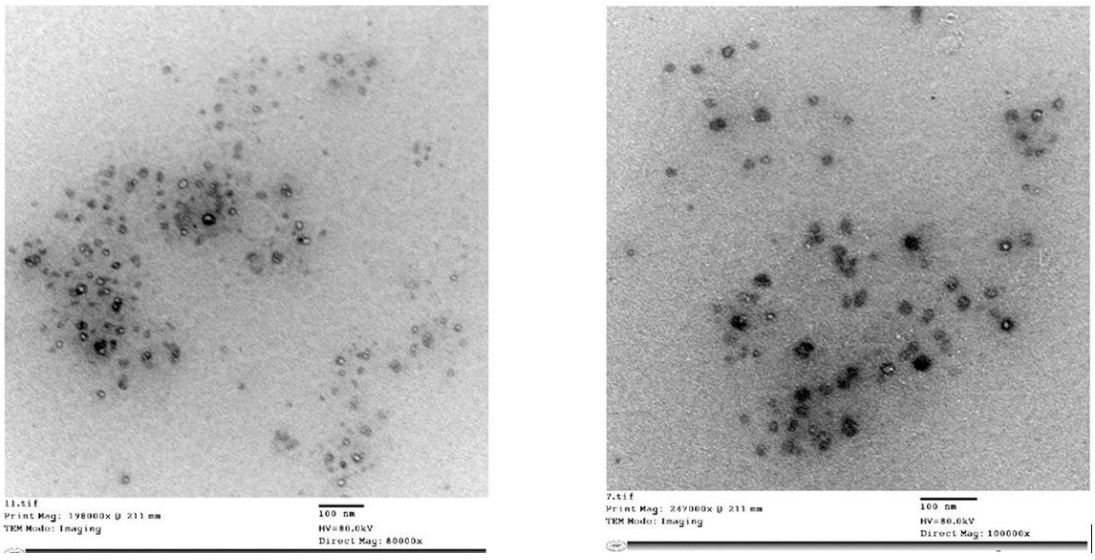

a) b)

Figure 3. TEM images of the optimized S6 formulation.

The cytotoxic activity of S6 was evaluated against MCF-7 breast cancer cells. Serial dilutions of S6, free Nitrofurantoin, and unloaded cubosomes were tested to assess their effects on cell viability. **Figure 4** presents the

percentage of viable cells for S6 in comparison to free NITRO and the unloaded cubosomes across the tested concentration range.

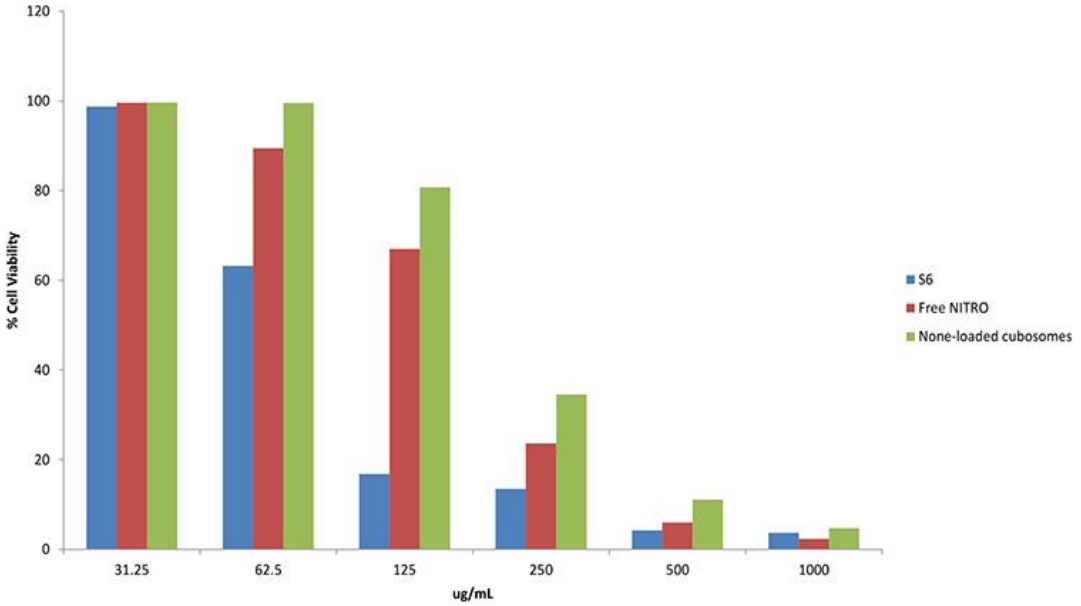

Figure 4. Impact of various dilutions of S6, free Nitrofurantoin, and unloaded cubosomes on MCF-7 cell viability.

The results indicate that S6 exhibits a markedly stronger cytotoxic effect compared to both free NITRO and the unloaded cubosomes. IC_{50} calculations confirmed that S6 achieves effective cell inhibition at lower concentrations, as illustrated in **Figure 5**.

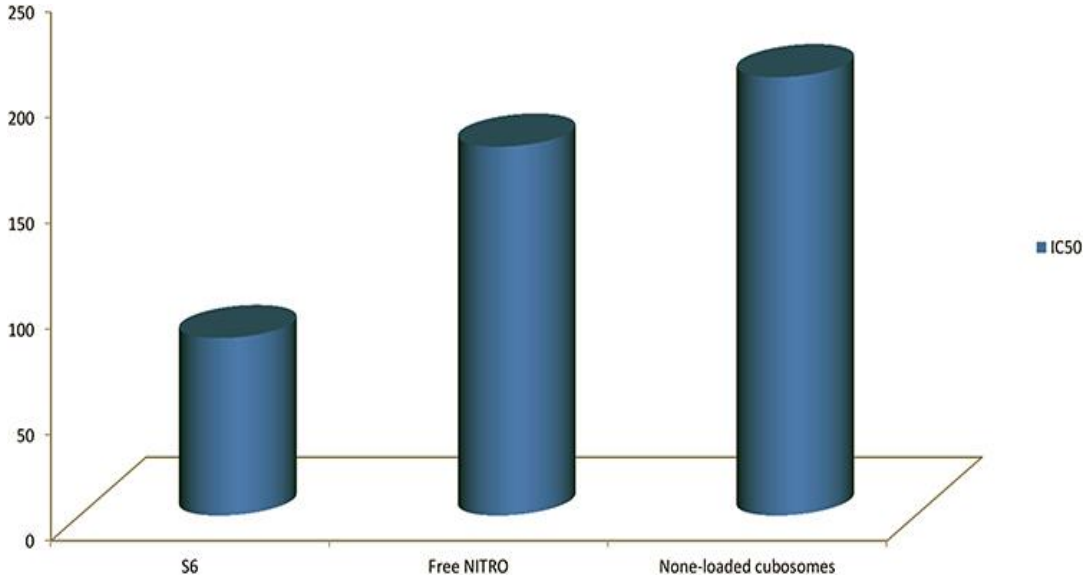

Figure 5. IC50 values for S6 in comparison to free NITRO and None-loaded Cubosomes.

ANOVA analysis indicated that S6 exhibited a significantly lower IC50 (83.99 ± 0.15 µg/mL) than Free NITRO (174.54 ± 1.36 µg/mL) and None-loaded Cubosomes (207.38 ± 0.59 µg/mL) ($p = 0.000$). The impact of S6, free NITRO, and None-loaded Cubosomes on cell viability was also evident in cell morphology relative to the control group, with **Figure 6** showing features of cellular stress, such as small, rounded cells.

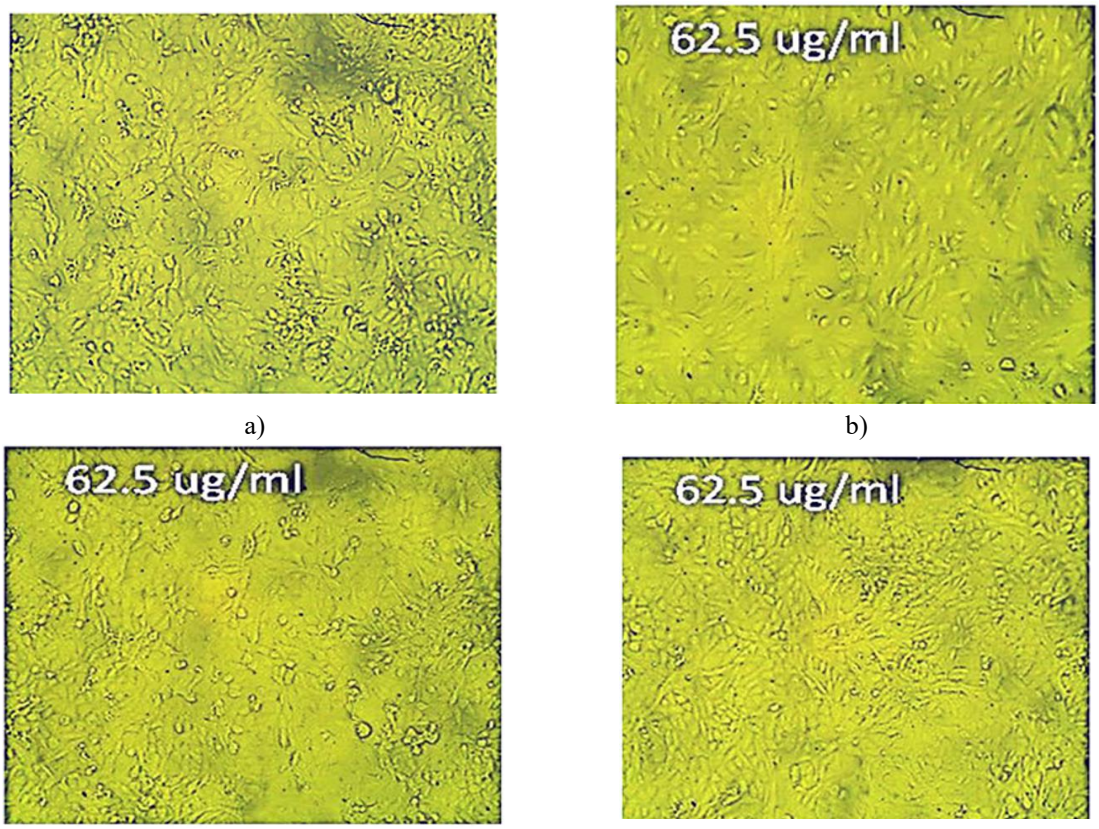

Figure 6. Inverted microscope images of (a) control MCF-7 cells, (b) cells treated with 62.5 µg/mL of S6, (c) cells exposed to Free NITRO, and (d) cells treated with None-loaded Cubosomes.

As presented in **Table 2**, all NITRO-Cs formulations demonstrated high encapsulation efficiency (%EE), ranging from 97.43% to 98.71%. ANOVA analysis indicated that higher %EE correlated with elevated oily: aqueous phase ratios and higher GMO:PX407 ratios ($p = 0.0007$), which was attributed to the poor water solubility of NITRO, causing the drug to be incorporated into the oily bilayer of GMO regardless of the relative amounts of GMO or water [52, 53]. Increasing the particle size (PS) corresponded with higher drug loading, consistent with prior findings for Flurbiprofen cubosomes [54]. Although higher PX407 percentages (lower GMO:PX407 ratio) tended to reduce PS, excessive PX407 could lead to the formation of alternative vesicular structures alongside cubosomes, explaining the relatively broad size distribution (PDI) observed with low GMO:PX407 ratios [55].

All formulations exhibited negative zeta potential (ZP), attributed to the negatively charged free oleic acid in GMO [56], and higher ZP values were linked to higher GMO content (high GMO:PX407 ratio), consistent with reports on Resveratrol cubosomes [57]. Desirability analysis identified S6 as the optimized system, which was subsequently evaluated for drug release, TEM imaging, and cytotoxicity.

The release profile of Free NITRO and S6 **(Figure 2)** demonstrated significantly higher drug release from S6 at 4 hours ($p = 0.00055$) and 8 hours ($p = 0.000237$), likely due to PX407 enhancing NITRO solubility and facilitating its release from the cubosomes [58]. S6 exhibited a biphasic release pattern: an initial rapid release phase from the drug solubilized within the nano-sized oily structure, followed by a slower release phase due to diffusion through the cubosome's tortuous network, in agreement with previous Clopidogrel Bisulphate cubosome studies [27]. Zero-order kinetics from S6 ensured a consistent drug delivery rate over time [59].

MCF-7 cell studies confirmed that NITRO could penetrate cells and induce cytotoxicity, both as free drug and within cubosomes. NITRO's mechanism involves activation by Nitro reductases into reactive intermediates that bind ribosomal proteins, inhibiting protein synthesis and damaging cells [20]. Since breast cancer cells overexpress Nitro reductase [60], NITRO in proximity to these cells was efficiently activated, explaining its inhibitory effect. S6 showed superior cytotoxicity to Free NITRO, with a significantly lower IC50 (83.99 ± 0.15 µg/mL vs. 174.54 ± 1.36 µg/mL), likely due to cubosome encapsulation, small particle size, and enhanced membrane permeation [28, 31]. None-loaded Cubosomes displayed minimal cytotoxicity, with a high IC50 (207.38 ± 0.59 µg/mL), confirming their biocompatibility at the effective S6 concentration [61].

Conclusion

These results indicate that the established antibiotic NITRO, commonly used for urinary tract infections, can be repurposed for cancer therapy through cubosome encapsulation, which enhances solubility and cellular uptake. NITRO cubosomes were formulated via hot homogenization using a 2^3 full factorial design, with S6 (1:10 drug: oily phase, 1:5 oily: aqueous phase, 0.5:1 GMO:PX407) showing optimal desirability. In this cubosomal system, NITRO exhibited cytotoxic effects against breast cancer cells through activation by cancer cell-expressed Nitro reductase and improved penetration facilitated by the cubosome carrier, while maintaining safety for normal cells. Therefore, NITRO has potential as a breast cancer therapeutic, aligning with sustainable development goals, and further in vivo and stability studies are recommended.

Acknowledgments: None

Conflict of Interest: None

Financial Support: None

Ethics Statement: None

References

1. Mansoori B, Mohammadi A, Davudian S, Shirjang S, Baradaran B. The different mechanisms of cancer drug resistance: a brief review. Adv Pharm Bull. 2017;7(3):339–48. doi:10.15171/apb.2017.041
2. Anand U, Dey A, Chandel AKS, Sanyal R, Mishra A, Pandey DK, et al. Cancer chemotherapy and beyond: current status, drug candidates, associated risks and progress in targeted therapeutics. Genes Dis. 2022;10(4):1367-401. doi:10.1016/j.gendis.2022.02.007. Erratum in: genes dis. 2024;11(4):101211. doi:10.1016/j.gendis.2024.1012113
3. Debela DT, Muzazu SG, Heraro KD, Ndalama MT, Mesele BW, Haile DC, et al. New approaches and procedures for cancer treatment: current perspectives. SAGE Open Med. 2021;9:20503121211034366. doi:10.1177/20503121211034366
4. Chupradit S, Widjaja G, Radhi Majeed B, Kuznetsova M, Ansari MJ, Suksatan W, et al. Recent advances in cold atmospheric plasma (CAP) for breast cancer therapy. Cell Biol Int. 2023;47(2):327-40. doi:10.1002/cbin.11939
5. Moura C, Correia AS, Pereira M, Ribeiro E, Santos J, Vale N. Atorvastatin and nitrofurantoin repurposed in the context of breast cancer and neuroblastoma cells. Biomedicines. 2023;11(3):903–23. doi:10.3390/biomedicines11030903
6. Rabelo ACS, Guerreiro CA, Shinzato VI, Ong TP, Noratto G. Anthocyanins reduce cell invasion and migration through akt/mtor downregulation and apoptosis activation in triple-negative breast cancer cells: a systematic review and meta-analysis. Cancers. 2023;15(18):2300–13. doi:10.3390/cancers15082300
7. El-Tanani M, Platt-Higgins A, Lee YF, Al Khatib AO, Haggag Y, Sutherland M, et al. Matrix metalloproteinase 2 is a target of the RAN-GTP pathway and mediates migration, invasion and metastasis in human breast cancer. Life Sci. 2022;310:121046. doi:10.1016/j.lfs.2022.121046
8. Guo Z, Zhang H, Fu Y, Kuang J, Zhao B, Zhang L, et al. Cancer-associated fibroblasts induce growth and radioresistance of breast cancer cells through paracrine IL-6. Cell Death Discov. 2023;9(1):6. doi:10.1038/s41420-023-01306-3
9. Hernandes EP, Lazarin-Bidóia D, Bini RD, Nakamura CV, Cótica LF, de Oliveira Silva Lautenschlager S. Doxorubicin-loaded iron oxide nanoparticles induce oxidative stress and cell cycle arrest in breast cancer cells. Antioxidants. 2023;12(2):273–89. doi:10.3390/antiox12020237
10. Ashrafizadeh M, Zarrabi A, Bigham A, Taheriazam A, Saghari Y, Mirzaei S, et al. (Nano)platforms in breast cancer therapy: drug/gene delivery, advanced nanocarriers and immunotherapy. Med Res Rev. 2023;43(6):2115-76. doi: 10.1002/med.21971
11. Yang F, He Q, Dai X, Zhang X, Song D. The potential role of nanomedicine in the treatment of breast cancer to overcome the obstacles of current therapies. Front Pharmacol. 2023;14(1):1–12.

12. Dongsar TT, Dongsar TS, Abourehab MA, Gupta N, Kesharwani P. Emerging application of magnetic nanoparticles for breast cancer therapy. Eur Polym J. 2023;187(1):1–10. doi:10.1016/j.eurpolymj.2023.111898
13. Rajaei M, Rashedi H, Yazdian F, Navaei-Nigjeh M, Rahdar A, Díez-Pascual AM. Chitosan/agarose/graphene oxide nanohydrogel as drug delivery system of 5-fluorouracil in breast cancer therapy. J Drug Deliv Sci Technol. 2023;82(1):1–10.
14. Xu J, Lai Y, Wang F, Zou Z, Pei R, Yu H, et al. Dual stimuli-activatable versatile nanoplatform for photodynamic therapy and chemotherapy of triple-negative breast cancer. Chinese Chem Lett. 2023;34(12):108332.
15. Taha S, Mohamed WR, Elhemely MA, El-Gendy AO, Mohamed T. Tunable femtosecond laser suppresses the proliferation of breast cancer in vitro. J Photochem Photobiol B: Biol. 2023;240(1):1–8. doi:10.1016/j.jphotobiol.2023.112665
16. Sleire L, Førde HE, Netland IA, Leiss L, Skeie BS, Enger PØ. Drug repurposing in cancer. Pharmacol Res. 2017;124(1):74–91. doi:10.1016/j.phrs.2017.07.013
17. Crofts TS, Sontha P, King AO, Wang B, Biddy BA, Zanolli N, et al. Discovery and characterization of a nitroreductase capable of conferring bacterial resistance to chloramphenicol. Cell Chem Biol. 2019;26(4):559-70.
18. Andrade JK, Souza MI, Gomes Filho MA, Silva DM, Barros AL, Rodrigues MD, et al. N-pentyl-nitrofurantoin induces apoptosis in HL-60 leukemia cell line by upregulating BAX and downregulating BCL-xL gene expression. Pharmacol Rep. 2016;68(5):1046-53.
19. Race PR, Lovering AL, Green RM, Ossor A, White SA, Searle PF, et al. Structural and mechanistic studies of Escherichia coli nitroreductase with the antibiotic nitrofurazone: Reversed binding orientations in different redox states of the enzyme. J Biol Chem. 2005;280(14):13256-64.
20. Wang Y, Gray JP, Mishin V, Heck DE, Laskin DL, Laskin JD. Role of cytochrome P450 reductase in nitrofurantoin-induced redox cycling and cytotoxicity. Free Radic Biol Med. 2008;44(6):1169–79. doi:10.1016/j.freeradbiomed.2007.12.013
21. Al-Masoudi NA, Al-Soud YA, Kalogerakis A, Pannecouque C, De Clercq E. Nitroimidazoles, part 2: synthesis, antiviral and antitumor activity of new 4- nitroimidazoles. Chem Biodivers. 2006;3(5):515–26. doi:10.1002/cbdv.200690055
22. Chen Z, Han F, Du Y, Shi H, Zhou W. Hypoxic microenvironment in cancer: molecular mechanisms and therapeutic interventions. Signal Transduct Target Ther. 2023;8(1):70–82. doi:10.1038/s41392-023-01332-8
23. Manin AN, Voronin AP, Boycov DE, Drozd KV, Churakov AV, Perlovich GL. A combination of virtual and experimental screening tools for the prediction of nitrofurantoin multicomponent crystals with pyridine derivatives. Crystals. 2023;13(7):1022. doi:10.3390/cryst13071022
24. Dadwal A, Baldi A, Kumar Narang R. Nanoparticles as carriers for drug delivery in cancer. Artif Cells Nanomed Biotechnol. 2018;46(1):295–305. doi:10.1080/21691401.2018.1457039
25. Yao Y, Zhou Y, Liu L, Xu Y, Chen Q, Wang Y, et al. Nanoparticle-based drug delivery in cancer therapy and its role in overcoming drug resistance. Front Mol Biosci. 2020;7:193. doi:10.3389/fmolb.2020.00193
26. Khan R, Arshad F, Hassan IU, Naikoo GA, Pedram MZ, Zedegan MS, et al. Advances in nanomaterial-based immunosensors for prostate cancer screening. Biomed Pharmacother. 2022;155:113649. doi:10.1016/j.biopha.2022.113649
27. El-Laithy H, Badawi A, Abdelmalak NS, El-Sayyad N. Cubosomes as oral drug delivery systems: a promising approach for enhancing the release of clopidogrel bisulphate in the intestine. Chem Pharm Bull. 2018;66(12):1165–73. doi:10.1248/cpb.c18-00615
28. Varghese R, Salvi S, Sood P, Kulkarni B, Kumar D. Cubosomes in cancer drug delivery: a review. Colloids Interface Sci Commun. 2022;46(1):1–11. doi:10.1016/j.colcom.2021.100561
29. Garg G, Saraf S, Saraf S. Cubosomes: an overview. Biol Pharm Bull. 2007;30(1):350–3. doi:10.1248/bpb.30.350
30. Shetty S, Shetty S. Cubosome-based cosmeceuticals: a breakthrough in skincare. Drug Discov Today. 2023;28(7):103623. doi:10.1016/j.drudis.2023.103623
31. Zhang L, Li J, Tian D, Sun L, Wang X, Tian M. Theranostic combinatorial drug-loaded coated cubosomes for enhanced tar geting and efficacy against cancer cells. Cell Death Dis. 2020;11(1):1.

32. Murgia S, Falchi AM, Mano M, Lampis S, Angius R, Carnerup AM, et al. Nanoparticles from lipid-based liquid crystals: emulsifier influence on morphology and cytotoxicity. J Phys Chem B. 2010;114(10):3518-25. doi:10.1021/jp9098655
33. Yaghmur A, Glatter O. Characterization and potential applications of nanostructured aqueous dispersions. Adv Colloid Interface Sci. 2009;147-148(1):333–42. doi:10.1016/j.cis.2008.07.007
34. Janakiraman K, Krishnaswami V, Sethuraman V, Rajendran V, Kandasamy R. Development of methotrexate-loaded cubosomes with improved skin permeation for the topical treatment of rheumatoid arthritis. Appl Nanosci. 2019;9(3):1781–96. doi:10.1007/s13204-019-00976-9
35. Madheswaran T, Kandasamy M, Bose R, Karuppagounder V. Current potential and challenges in the advances of liquid crystalline nanoparticles as drug delivery systems. Drug Discov Today. 2019;24(7):1405-12. doi:10.1016/j.drudis.2019.05.004
36. Lars L, Sandra W, Ajay Vikram S, Peter L, Andreas L. Nanoparticle induced barrier function assessment at liquid–liquid and air–liquid interface in novel human lung epithelia cell lines. Toxicol Res. 2019;8(1):1016–27. doi:10.1039/c9tx00179d
37. Sivadasan D, Sultan MH, Alqahtani SS, Javed S. Cubosomes in drug delivery—a comprehensive review on its structural componen ts, preparation techniques and therapeutic applications. Biomedicines. 2023;11(4):1114–39. doi:10.3390/biomedicines11041114
38. Siekmann B, Bunjes H, Koch MH, Westesen K. Preparation and structural investigations of colloidal dispersions prepared from cubic monoglyceride water phases. Int J Pharm. 2002;244(1–2):33–43. doi:10.1016/S0378-5173(02)00298-3
39. Meli V, Caltagirone C, Falchi AM, Hyde ST, Lippolis V, Monduzzi M, et al. Docetaxel-loaded fluorescent liquid-crystalline nanoparticles for cancer theranostics. Langmuir ACS J Surf Colloids. 2015;31(35):9566–75. doi:10.1021/acs.langmuir.5b02101
40. Salema EM, Dawabaa HM, Gadc S, Hassanc TH. Cubosomes as an Oral Drug Delivery System. Rec Pharm Biomed Sci. 2023;7(3):81–90.
41. Umar HA, Wahab H, Gazzali AM, Tahir H, Ahmed W. Cubosomes: design, development, and tumor-targeted drug delivery applications. Polymers (Basel). 2022;14(15):3118–36. doi:10.3390/polym14153118
42. El-Hashemy HA, Salama A, Rashad A. Experimental design, formulation, and in-vivo evaluation of novel anticoagulant Rivaroxaban loaded cubosomes in rats model. J Liposome Res. 2022;1(1):1–8.
43. Zewail M, Gaafar PME, Ali MM, Abbasa H. Lipidic cubic-phase leflunomide nanoparticles (cubosomes) as a potential tool for breast cancer management. Drug Deliv. 2022;29(1):1663–74. doi:10.1080/10717544.2022.2079770
44. Nasr M, Younes H, Abdel-Rashid RS. Formulation and evaluation of cubosomes containing colchicine for transdermal delivery. Drug Deliv Transl Res. 2020;10(1):1302–13. doi:10.1007/s13346-020-00785-6
45. Cair MR, Pienaar EW, Lotter AP. Polymorphism and pseudopolymorphism of the antibacterial nitrofurantoin. Mol Cryst Liq Cryst. 1996;279(1):241–64. doi:10.1080/10587259608042194
46. Marques C, Maurizi L, Borchard G, Jordan O. Characterization challenges of self-assembled polymer-SPIONs nanoparticles: benefits of orthogonal methods. Int J Mol Sci. 2022;23(1):1–17. doi:10.3390/ijms232416124
47. Hashem F, Nasr M, Youssif M. Formulation and characterization of cubosomes containing REB for improvement of oral absorption of the drug in human volunteers. J Adv Pharm Res. 2018;2(2):95–103. doi:10.21608/aprh.2018.5828
48. Elsayad M, Mowafy HA, Zaky AA, Samy AA. Chitosan caged liposomes for improving oral bioavailability of rivaroxaban: in vitro and in vivo evaluation. Pharm Dev Technol. 2021;26(3):316–27. doi:10.1080/10837450.2020.1870237
49. Chettupalli AK, Ananthula M, Amarachinta PR, Bakshi V, Yata VK. Design, formulation, in-vitro and ex-vivo evaluation of atazanavir loaded cubosomal gel. Biointerface Res Appl Chem. 2021;11(4):12037–54.
50. Kamel AA, Fadel M, Louis D. Curcumin-loaded nanostructured lipid carriers prepared using Peceol™ and olive oil in photodynamic therapy: development and application in breast cancer cell line. Int J Nanomed. 2019;14(1):5073–85. doi:10.2147/IJN.S210484
51. Shah M, Pathak K. Development and statistical optimization of solid lipid nanoparticles of simvastatin by using 23 full-factorial design. AAPS Pharm Sci Tech. 2010;11(2):489–96. doi:10.1208/s12249-010-9414-z

52. Flak DK, Adamski V, Nowaczyk G, Szutkowski K, Synowitz M, Jurga S, et al. AT101-Loaded cubosomes as an alternative for improved glioblastoma therapy. Int J Nanomed. 2020;15:7415–31. doi:10.2147/IJN.S265061
53. Segalina A, Pavan B, Ferretti V, Spizzo F, Botti G, Bianchi A, et al. Cocrystals of nitrofurantoin: how coformers can modify its solubility and permeability across intestinal cell monolayers. Crystal Growth Des. 2022;22(5):3090-106.
54. Han S, Shen JQ, Gan Y, Geng HM, Zhang XX, Zhu CL, et al. Novel vehicle based on cubosomes for ophthalmic delivery of flurbiprofen with low irritancy and high bioavailability. Acta Pharmacol Sin. 2010;31(8):990-8.
55. Nasr M, Ghorab MK, A A. In vitro and in vivo evaluation of cubosomes containing 5-fluorouracil for liver targeting. Acta Pharm Sin B. 2015;5(1):79–88. doi:10.1016/j.apsb.2014.12.001
56. Hakim E, El-Mahrouk GM, Abdelbary G, Teaima MH. Freeze-dried clopidogrel loaded lyotropic liquid crystal: box-behnken optimization, in-vitro and in-vivo evaluation. Curr Drug Deliv. 2020;17(3):207–17. doi:10.2174/1567201817666200122161433
57. Abdel-Bar HM, Sanad RA. Endocytic pathways of optimized resveratrol cubosomes capturing into human hepatoma cells. Biomed Pharmacother. 2017;93(1):561–9. doi:10.1016/j.biopha.2017.06.093
58. Zaki RM, Abou El Ela AE, Almurshedi AS, Aldosari BN, Aldossari AA, Ibrahim MA. Fabrication and assessment of orodispersible tablets loaded with cubosomes for the improved anticancer activity of simvastatin against the MDA-MB-231 breast cancer cell line. Polymers. 2023;15(7):1774–88. doi:10.3390/polym15071774
59. Adepu S, Ramakrishna S. Controlled drug delivery systems: current status and future directions. Molecules. 2021;26(19):1–45. doi:10.3390/molecules26195905
60. Lu SB, Wei L, He W, Bi ZY, Qian Y, Wang J, et al. Recent advances in the enzyme-activatable organic fluorescent probes for tumor imaging and therapy. ChemistryOpen. 2022;11(10):202200137.
61. Almoshari Y, Alam MI, Bakkari MA, Salawi A, Alshamrani M, Sabei FY, et al. Formulation, characterization, and evaluation of doxorubicin-loaded cubosome as a cytotoxic potentiator against HCT-116 colorectal cancer cells. Indian J Pharm Educ Res. 2022;56(3):723-31.